

# Time-domain spectroscopy of optical parametric amplification for phase-stable terahertz-to-midinfrared pulses

NATSUKI KANDA,<sup>1,\*</sup> NOBUHISA ISHII,<sup>1,2</sup> JIRO ITATANI<sup>1</sup> AND RYUSUKE MATSUNAGA<sup>1,3</sup>

<sup>1</sup>The Institute for Solid State Physics, The University of Tokyo, Kashiwa, Chiba 277-8581, Japan.

<sup>2</sup>Kansai Photon Science Institute, National Institutes for Quantum and Radiological Science and Technology (QST), Kyoto 619-0215, Japan

<sup>3</sup>PRESTO, Japan Science and Technology Agency, Saitama 332-0012, Japan.

\*[n-kanda@issp.u-tokyo.ac.jp](mailto:n-kanda@issp.u-tokyo.ac.jp)

**Abstract:** We demonstrate time-domain spectroscopy of terahertz (THz)-to-midinfrared (MIR) pulses up to around 50 THz frequency based on a highly-stable Yb:KGW regenerative amplifier with pulse duration of 255 fs. Intra-pulse difference frequency generation in a GaSe crystal with an 11-fs pulse compressed by a multi-plate broadening scheme realizes the excellent phase stability of the THz-to-MIR pulses, which is further amplified by optical parametric amplification (OPA). The OPA process is characterized in the time domain, showing the wide tunability in the unexplored low frequency region in 17.5-43.6 THz (6.9-17  $\mu\text{m}$ ) by rotating the nonlinear crystal. The long-term phase drift of the amplified signal is evaluated as small as 44 mrad in 6-hour operation without any active feedback. The demonstrated OPA scheme for the generation of waveform-controlled THz-to-MIR pulse will open a new route to ultrafast infrared science.

## 1. Introduction

Developments of intense ultrafast pulsed lasers and nonlinear optics have realized novel wavelength conversion to terahertz (THz) frequency for investigating low-frequency electromagnetic responses in various kinds of matters [1-6]. Mid-infrared (MIR) pulse generation by optical parametric amplification (OPA) is also important, *e.g.*, for higher-harmonic generation in gaseous system to generate coherent soft X-ray pulses for attosecond science [7]. More recently, the intermediate frequency between the THz (0.1-10 THz, wavelength  $>30 \mu\text{m}$ ) and the MIR (75-120 THz, or 2.5-4  $\mu\text{m}$ ) region, *i.e.*, from 10 to several tens of THz (4-30  $\mu\text{m}$ ), is attracting growing interests as a next frontier in ultrafast optical science from the following reasons: (i) Compared to THz frequency, the pulse energy can be more tightly confined both in time and space, which leads to much higher peak field exceeding several tens of MV/cm [8]. (ii) Since the photon energy is much lower than near-infrared (NIR) or visible range, intense light field can be applied in matter without damaging. (iii) Since the field cycle on the order of 10 fs is comparable to or even shorter than electron scattering times, both the coherent and incoherent interaction can be involved, resulting in the emergence of nontrivial dynamics of electrons as presented in higher-harmonic generation in solids [9,10]. Furthermore, (iv) many materials have eigenmodes of lattice vibrations, or phonons, in the THz-to-MIR frequency. This is also the reason why suitable light sources have been difficult to develop in this frequency range. Recent experiments have demonstrated the light-induced phase transition by strongly shaking the lattice vibrations with directly changing the atomic structure and symmetry, which opens a new research field for the dynamical control of materials [11-15]. For this purpose, in which the interaction is far beyond the perturbative regime, the time-domain waveform of the oscillating electric field essentially plays a key role. Therefore, intense light sources with stable carrier-envelope phase (CEP) are highly demanded.

Intense phase-locked THz-to-MIR pulses (10-70 THz) have been realized by differential frequency generation (DFG) in nonlinear crystals using two-color NIR laser pulses with the same carrier-envelope-offset frequency [8,16]. It has been also expanded for high repetition laser system [17] and broadband idler pulse generation [18,19]. Even in these novel schemes, however, the CEP of the output pulse can fluctuate in time due to long-term instability of the relative optical path length for the two different beams, leading to the requirement for an active feedback system to achieve the fluctuation as small as 100-200 mrad [20,21]. In this sense, intra-pulse DFG, *i.e.*, the DFG within a single broadband fundamental pulse, has a great advantage for the CEP stability because of the common path for every frequency, as in the very same way with optical rectification in conventional THz time-domain spectroscopy. If this CEP-locked output is further amplified afterward, generation of intense THz-to-MIR pulses would be realized with excellent stability of the field waveform. Such an amplification of the CEP-stabilized seed pulses has been used in, *e.g.*, optical parametric chirped-pulse amplification in NIR region [22], and also recently in the MIR frequency between 2.7-3.8  $\mu\text{m}$  (80-110 THz) [23]. To the best of our knowledge, the amplification of further longer wavelength has not been reported thus far due to the concern of low efficiency for the small photon energy.

Here, we demonstrate the generation of a phase-stable seed pulse in the THz-to-MIR region (10-70 THz) by intra-pulse DFG and its amplification. Output of an Yb-based amplified laser with pulse duration of 255 fs is compressed to 11 fs by the multi-plate broadening scheme [23-27]. The compressed pulses are used for intra-pulse DFG in a thin GaSe plate to perform broadband time-domain spectroscopy up to 50 THz with the excellent phase stability. In addition, by using a thicker GaSe crystal with optimized phase-match condition, generation of frequency-tunable THz-to-MIR pulse and its amplification are also presented between 17.5-43.6 THz (6.9-17  $\mu\text{m}$ ). The excellent phase stability of the amplified pulses, fluctuating only 44 mrad in several hours without any active feedback, allows us to visualize the OPA process in time domain. Our demonstration of the simple and stable scheme for the pulse compression and intra-pulse DFG with following OPA in this THz-to-MIR frequency opens a new route to achieve a phase-stable light source for time-domain spectroscopy and promising further amplification for intense light field.

## 2. Multi-plate pulse compression and intra-pulse DFG

We started from a Yb:KGW regenerative amplifier (PHAROS PH1-2mJ, Light Conversion, UAB) with the pulse energy of 2 mJ, the repetition rate of 3 kHz, the pulse duration of 255 fs, and the center wavelength of 1028 nm. Since Yb-based lasers can be directly pumped by laser diodes with high quantum efficiency, the output is so stable as the shot-by-shot pulse energy fluctuation is less than 0.04 % in the standard deviation with high repetition rate. Therefore, it is now being widely used in spite of relatively-longer pulse duration (150-300 fs). To generate the THz-to-MIR seed pulse by intra-pulse DFG, a short pulse around 10 fs is required. As the spectral broadening and pulse compression techniques, white-light generation in a single crystal [28] and gas-based hollow-core fiber [29,30] or filamentation have been developed well in the past few decades. However, the former is limited for a weak pulse less than a few  $\mu\text{J}$  since for a stronger pulse the multi-filamentation and the optical damage in the crystal crucially degrade the beam quality. The latter method, on the other hand, requires an intense millijoule pulse energy because of the threshold of the spectral broadening in a gas phase. Very recently, another compression scheme has been proposed to realize the pulse compression for the moderate pulse energy (10  $\mu\text{J}$ -sub mJ) by using a series of thin plate [24-27]. Here we performed this multi-plate pulse compression (MPC) method for a part of the output with pulse energy of 215  $\mu\text{J}$ , as shown in Fig. 1(a). In order to obtain sufficient bandwidth two-stage MPC is employed similarly with our previous work [23], while original pulse duration is slightly longer in this work. The pulse is loosely focused onto fused silica plates with their Brewster angle to avoid

surface reflection loss. If a nonlinear thick crystal is placed too closely to the focal point, multi-filaments would be generated in the medium and the beam profile would be significantly deformed, then the pulse cannot propagate with keeping the profile nor be compressed to a short pulse by lower order dispersion compensation. For a thin plate moderately placed closely to the focal point, however, the beam profile shows concentration into the central part by the optical Kerr effect, in which the spectrum is broadened, with another concentric outer-ring profile where the spectrum is almost unchanged. By placing the plate properly so as to show the concentric multi-ring shape, the divergence of the beam and the collimation with the Kerr-lens effect are balanced and then the self-focusing of the beam occurs again. Thus, one can repeat the spectral broadening by using many thin plates with effectively large interaction length.

At the first stage of MPC, four 2-mm-thick plates and two 1-mm-thick plates are used, and only the central part of the beam with nearly uniform profile and efficient spectra broadening is depicted with an aperture. Then the dispersion is compensated by 6-time reflections of Gires-Tournois interferometer (GTI) mirrors whose negative group delay dispersion is  $-550 \text{ fs}^2$  (101645, Layertec GmbH). After the compression in the first stage, the pulse duration is 66 fs with the pulse energy of 73  $\mu\text{J}$ . The throughput of the first stage is  $\sim 34\%$  that is limited by the aperture. At the second stage, six 2-mm-thick plates are used for broadening, and the pulse is compressed by 6-time reflections of a pair of chirp mirrors (Tokai Optical Co. Ltd.) with negative group delay dispersion of  $-100 \text{ fs}^2$  per reflection in pair. The output pulse energy is 27  $\mu\text{J}$ , and the throughput of the second stage and whole compression is  $\sim 37\%$  and  $\sim 13\%$ , respectively. Note that the group delay dispersion of the output from multi-plates is over-compensated for a following setup of time-domain spectroscopy which contains transmission in a beam splitter with positive chirp. Some thinner fused silica plates are inserted to minimize the pulse duration at the nonlinear crystal positions for generation and detection of THz-MIR field.

Figure 1(b) shows the distribution of the output pulse energy measured by a photodiode. Remarkably, the shot-by-shot pulse energy fluctuation is as small as 0.05% in the standard deviation even for the nonlinear spectral broadening and compression, which corroborates the stability of this compression method available for a variety of optical systems. The compressed pulse is characterized with second harmonic generation-based frequency resolved optical gating (SHG-FROG) method, as shown in Fig. 1(c). Figures 1(d) and 1(e) show the retrieved intensity and phase spectra, and time-domain waveform of the pulse envelope. The intensity spectrum is broad enough for generation of several tens of THz pulse with intra-pulse DFG, and the compressed pulse duration is as short as 11 fs which is close to Fourier-transform-limited.

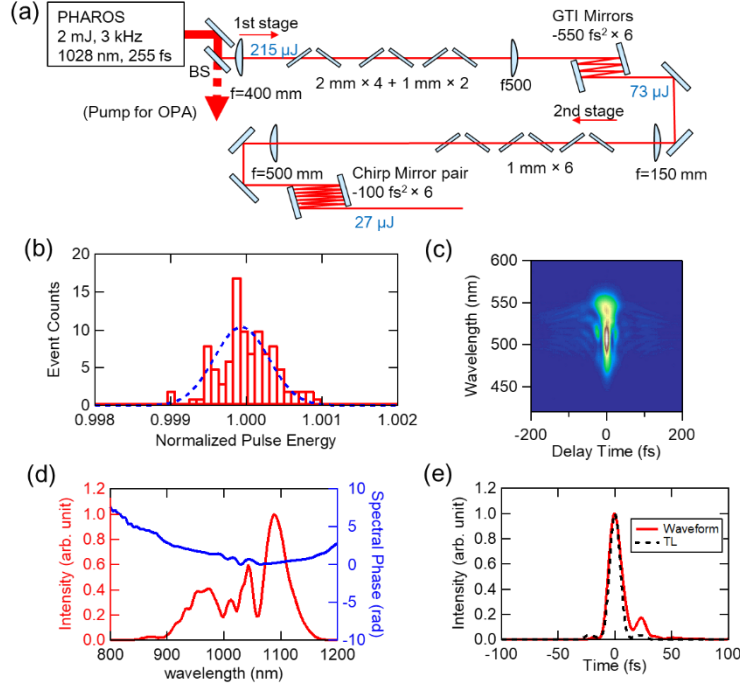


Fig. 1: Multi-plate spectral broadening and pulse compression. (a) A schematic of the setup consisted of two stages of broadening and compression. (b) Histogram of the output pulse energy measured with shot-by-shot detection (red). Normal distribution function with standard deviation of 0.05% is also shown (blue). (c) SHG-FROG trace of the output of the 2nd stage compression. (d) Retrieved intensity spectrum (red) and spectral phase (blue). (e) Time-domain intensity envelope of the retrieved pulse (red solid) and Fourier-transform-limited pulse (black dashed).

By using this stable compressed pulse, we perform THz-to-MIR time-domain spectroscopy. Broadband THz-to-MIR pulse is generated by intra-pulse DFG in a *c*-axis cleaved GaSe crystals with the thickness of 14  $\mu\text{m}$ . Another thin GaSe crystal with the thickness of 3.5  $\mu\text{m}$  is used for the detection of the THz-MIR pulse with the electro-optic sampling (EOS) method with a gate pulse. By using these thin crystals, a broadband pulse can be generated and detected without being restricted by the phase match condition [31-34]. The emitted THz-to-MIR beam is collimated and focused with off-axis parabolic mirrors to the detection crystal. The area of the THz-to-MIR pulse propagation is purged with dry Nitrogen to remove the absorption of  $\text{H}_2\text{O}$  and  $\text{CO}_2$ . Figures 2(a) and 2(b) show the time-domain waveform of the electric field and the power spectrum, respectively, indicating the short waveform and broad power spectrum up to 50 THz. Figure 2(c) shows the two-dimensional plot of the time-domain waveforms repeatedly measured in 6 hours. From this data the timing jitter is evaluated as less than 1 fs and long-term analyzed CEP stability of 35 mrad in the standard deviation. The result shows the remarkable stability of the field waveform without any feedback owing to the intra-pulse DFG process and would be utilized for practical application in the time-domain spectroscopy up to 50 THz.

We also use a thick GaSe crystal to increase the THz-to-MIR pulse intensity. Here we have to satisfy the type-II phase matching;  $\omega_1(e) + \omega_2(o) \rightarrow \Omega = \omega_1 - \omega_2(o)$ , where  $\omega_1$  and  $\omega_2$  are the frequency in NIR contained in the fundamental pulse and  $\Omega$  is the DFG frequency. By changing

the incident angle, the DFG frequency  $\Omega$  can be tuned according to the phase match condition [17,31,35]. Since the fundamental beam should contain both ordinary and extra-ordinary polarizations, the polarization of the compressed 11-fs pulse is rotated by 45 degrees with a half waveplate before the crystal. Figure 2(d) shows the power spectra with different incident angles. Here, a 0.5-mm-thick GaSe crystal and a 100- $\mu\text{m}$ -thick ZnTe crystal are used for generation and EOS, respectively. The generated frequency can be tuned from about 10 to 30 THz reflecting the phase-match condition of the GaSe crystal, which is consistent with the previous calculation [17].

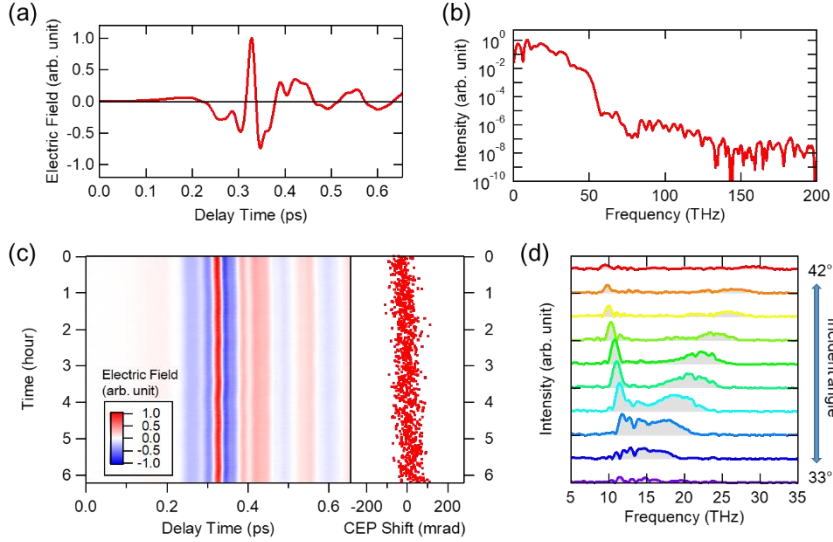


Fig. 2: (a)(b) Time-domain waveform and power spectrum of a broadband THz-to-MIR pulse generated by intra-pulse DFG with a thin GaSe crystal, respectively. (c) Stability of the waveform for more than 6 hours. Analyzed CEP shift is also shown in the right side. (d) Tunability of the power spectra for the narrowband THz-to-MIR pulse by intra-pulse DFG with 0.5-mm-thick GaSe crystal.

### 3. OPA in THz-MIR region

Here, we demonstrate amplification of the phase-stable THz-MIR pulse by OPA process, which is a key technology for generating intense light sources. Since OPA process is based on stimulated emission of a seed photon, the amplified light is expected to be also as stable as the seed pulse. Figure 3(a) shows the schematic of OPA demonstration. The THz-to-MIR pulse generated by intra-pulse DFG with a 1-mm-thick GaSe crystal in Fig. 2(d) is used as a seed, which is focused onto another 2-mm-thick GaSe crystal for OPA. The pump pulse with the pulse duration of 255 fs is separated before the MPC as shown in Fig. 1(a). Pulse energy of 277  $\mu\text{J}$  is used for the pump in this work. The phase match condition for the OPA are almost same with that of DFG because just the roles of  $\omega_2$  and  $\Omega$  are replaced. For the polarization selection rule, the seed and pump pulses are *s*- and *p*-polarizations on the OPA crystal, respectively. Finally, the transmitted field is detected by EOS with the gate pulse.

Figure 3(b) shows the output transmitted field waveforms at the pump delays of 0 and  $-10$  ps. Corresponding power spectra with the peak frequency of 17.7 THz are shown in Fig. 3(c). At the pump delay of  $-10$  ps, the seed pulse just passes through the crystal long before the pump (seed-first limit) comes in. At the pump delay of 0 ps, on the other hand, the pump and seed pulses temporally overlap, resulting in the enhancement of the seed as clearly observed. To the best of our knowledge, it might be the first observation of OPA as an electric field in time domain. Figure 3(d) shows two-dimensional plot of the output waveform with functions of the

gate delay and pump delay. The dashed line indicates the timing of the pump pulse entering the OPA crystal, around which the amplification is clearly observed. The upper-right and the lower-left sides of the dashed line correspond to the pump-first and seed-first conditions, respectively.

The integrated intensity and phase at the peak frequency as a function of the pump delay are also shown in the right side of Fig. 3(d). Intensity is normalized with that at the seed-first limit. The output intensity is amplified by more than 100 at around the zero pump delay, and then drastically decreases after the pump pulse passing through the crystal before the seed. It can be attributed to the absorption and screening of free carriers excited by the pump with multiphoton absorption. To confirm the validity of this interpretation, we also performed similar measurements with *s*-polarization pump, where the phase match condition is not satisfied. In this case, the amplification does not appear and only the depletion of the intensity in the pump-first condition is observed. The phase shift as large as 3 rad is also identified around the zero pump delay, which can be attributed to the screening and the change of the refractive index due to the photoexcitation of carriers.

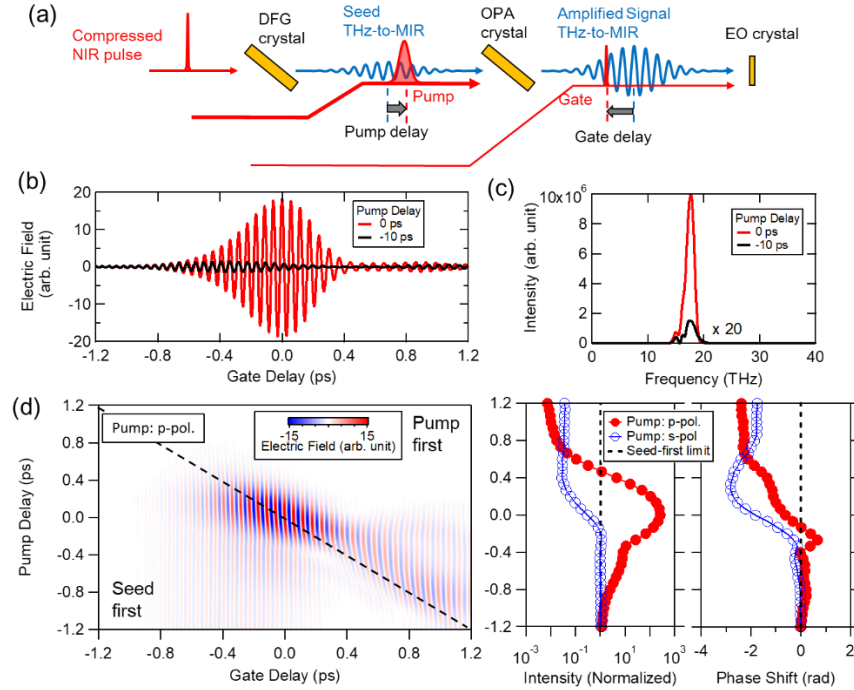


Fig. 3: (a) A schematic of time-resolved measurement of OPA dynamics. (b)(c) Time-domain waveforms and the power spectra of the transmitted THz-to-MIR pulse at zero pump delay (red) and the seed-first limit (pump delay of  $-10$  ps) (black). Note that the spectrum at the seed-first limit in (c) is magnified by 10 for visibility. (d) Two-dimensional plot of the time-domain waveforms for the amplified pulse with a function of the gate delay (horizontal) and the pump delay (vertical). In the right side, the pump-delay dependence of the integrated intensity (middle) and the phase (right) are shown with red markers. For comparison, the results with *s*-polarization are also shown with blue markers, where OPA does not occur.

Here we demonstrate the frequency tuning of this OPA. As shown in the intra-pulse DFG in Fig. 2(d), the peak frequency of the amplified signal can be tuned by changing the incident angle to the OPA crystal. The lower in Fig. 4(a) show the normalized spectra of the amplified pulse for different incident angles from 36 degrees to 50 degrees. The integrated intensities

with and without the pump are also shown in the upper of Fig. 4(a). The peak frequency can be tuned from 17.5 to 43.6 THz with amplification factor more than 10.

Finally, we also evaluate the long-term stability of the amplified THz-to-MIR pulse. Figure 4(b) show the two-dimensional plot of the time-domain waveform repeatedly measured in 6 hours. The phase shift of each measurement is shown in the right side. The fluctuation of phase is as small as 44 mrad in standard deviation without any active feedback. Such a high phase stability in the amplified pulse is realized owing to the intra-pulse DFG method in the generation of phase-stable seed pulse. The slight increase of the fluctuation compared to the seed in Fig. 2(c) can be attributed to the jitter between the seed and pump pulses, but it does not severely affect the phase stability in this OPA process.

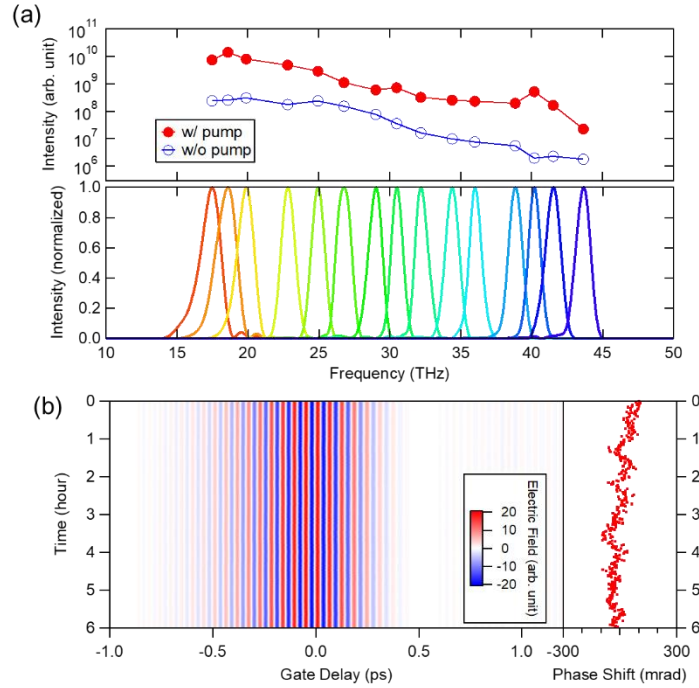


Fig. 4: (a) Tuning of OPA by changing the incident angle. Normalized power spectra from incident angles from 36 to 50 degrees (lower), and peak-frequency dependence of intensity with pump (red) and without the pump (blue) (upper). (b) Stability of the waveform of the amplified signal for 6 hours. Phase shift is also shown in the right side.

#### 4. Conclusion

We reported the time-domain spectroscopy of the phase-stable THz-to-MIR pulse with OPA in GaSe crystals. The multi-plate broadening scheme realizes the pulse compression for the Yb-based regenerative amplifier from 255 fs to 11 fs with shot-by-shot fluctuation less than 0.05 %. By using the 11-fs pulses for intra-pulse DFG, we demonstrated time-domain spectroscopy for the THz-to-MIR pulses up to 50 THz with the excellent phase stability fluctuating only 35 mrad in 6-hour operation. By using the THz-to-MIR pulse as the seed, we also demonstrated the time-domain OPA in the unexplored low-frequency region from 17.5 to 43.6 THz by tuning the incident angle to the GaSe crystal. The amplified signal is also quite stable as keeping the phase shift of 44 mrad in the standard deviation in 6-hour operation. Our method opens a new route for obtaining high-intensity and phase-stable THz-to-MIR light

source for infrared science without any active stabilization. Other nonlinear crystals such as  $\text{LiGaS}_2$  or  $\text{LiGaSe}_2$  are also hopeful for higher frequency region up to 60 THz [17,18,36]. Though we performed only the single-stage OPA in this work, this method can be extended to multi-stage OPA where much higher-intensity would be realized. Our time-domain study for the OPA process would also give us deeper insight for further optimizing the OPA output.

## Funding

This work was supported in part by JSPS KAKENHI (Grant No. JP19K15462, JP18H01843, JP19H02623, JP18H05250), JST PRESTO (Grant No. JPMJPR16PA), the Murata foundation, and MEXT Quantum Leap Flagship Program (MEXT Q-LEAP) Grant Number JPMXS0118068681.

## Disclosures

The authors declare no conflicts of interest.

## References

1. Yun-Shik Lee, "Principles of Terahertz Science and Technology," (Springer, 2008).
2. M. C. Beard, G. M. Turner, and C. A. Schmuttenmaer, "Terahertz spectroscopy". *J. Phys. Chem. B* **106**, 7146–7159 (2002).
3. T. Kampfrath, K. Tanaka, and K. A. Nelson, "Resonant and nonresonant control over matter and light by intense terahertz transients," *Nat. Photon.* **7**, 680-690 (2013).
4. T. Kampfrath, A. Sell, G. Klatt, A. Pashkin, S. Mährlein, T. Dekorsy, M. Wolf, M. Fiebig, A. Leitenstorfer and R. Huber, "Coherent terahertz control of antiferromagnetic spin waves," *Nat. Photonics* **5**, 31-34 (2011).
5. N. Kanda, T. Higuchi, H. Shimizu, K. Konishi, K. Yoshioka, and M. Kuwata-Gonokami, "The vectorial control of magnetization by light," *Nat. Commun.* **2**, 362 (2011).
6. R. Matsunaga, N. Tsuji, H. Fujita, A. Sugioka, K. Makise, Y. Uzawa, H. Terai, Z. Wang, H. Aoki, and R. Shimano, "Light-induced collective pseudospin precession resonating with Higgs mode in a superconductor," *Science* **345**, 1145-1149 (2014).
7. T. Popmintchev, M.-C. Chen, D. Popmintchev, P. Arpin, S. Brown, S. Ališauskas, G. Andriukaitis, T. Balciunas, O. D. Mücke, A. Pugzlys, A. Baltuška, B. Shim, S. E. Schrauth, A. Gaeta, C. Hernández-García, L. Plaja, A. Becker, A. Jaron-Becker, M. M. Murnane, and H. C. Kapteyn, "Bright coherent ultrahigh harmonics in the keV x-ray regime from mid-infrared femtosecond lasers," *Science* **336**, 1287–1291 (2012).
8. A. Sell, A. Leitenstorfer, and R. Huber, "Phase-locked generation and field-resolved detection of widely tunable terahertz pulses with amplitudes exceeding 100 MV/cm," *Opt. Lett.* **33**, 2767–2769 (2008).
9. S. Ghimire, A. D. DiChiara, E. Sistrunk, P. Agostini, L. F. DiMauro, and D. A. Reis, "Observation of high-order harmonic generation in a bulk crystal," *Nat. Phys.* **7**, 138–141 (2010).
10. O. Schubert, M. Hohenleutner, F. Langer, B. Urbanek, C. Lange, U. Huttner, D. Golde, T. Meier, M. Kira, S. W. Koch, and R. Huber, "Sub-cycle control of terahertz high-harmonic generation by dynamical Bloch oscillations," *Nat. Photonics* **8**, 119–123 (2014).
11. M. Mitrano, A. Cantaluppi, D. Nicoletti, S. Kaiser, A. Perucchi, S. Lupi, P. Di Pietro, D. Pontiroli, M. Riccò, S. R. Clark, D. Jaksch, and A. Cavalleri, "Possible light-induced superconductivity in  $\text{K}_3\text{C}_60$  at high temperature," *Nature* **530**, 461 (2016).
12. R. Mankowsky, A. von Hoegen, M. Först, and A. Cavalleri, *Phys. Rev. Lett.* **118**, 197601 (2017).
13. X. Li, T. Qiu, J. Zhang, E. Baldini, J. Lu, A. M. Rappe, K. A. Nelson, "Terahertz field-induced ferroelectricity in quantum paraelectric  $\text{SrTiO}_3$ ," *Science* **364**, 1079 (2019).
14. E. J. Sie, C. M. Nyby, C. D. Pemmaraju, S. J. Park, X. Shen, J. Yang, M. C. Hoffmann, B. K. Ofori-Okai, R. Li, A. H. Reid, S. Weathersby, E. Mannebach, N. Finney, D. Rhodes, D. Chenet, A. Antony, L. Balicas, J. Hone, T.P. Devereaux, T. F. Heinz, X. Wang, and A. M. Lindenberg, "An ultrafast symmetry switch in a Weyl semimetal," *Nature* **565**, 61 (2019).
15. M. Rini, R. Tobey, N. Dean, J. Itatani, Y. Tomioka, Y. Tokura, R. W. Schoenlein, and A. Cavalleri, "Control of the electronic phase of a manganite by mode-selective vibrational excitation," *Nature* **449**, 72–74(2007).
16. B. Liu, H. Bromberger, A. Cartella, T. Gebert, M. Först, and A. Cavalleri, "Generation of narrowband, high-intensity, carrier-envelope phase-stable pulses tunable between 4 and 18 THz," *Opt. Lett.* **42**, 129–131 (2017).
17. M. Knorr, J. Raab, M. Tauer, P. Merkl, D. Peller, E. Wittmann, E. Riedle, C. Lange, and R. Huber, "Phase-locked multi-terahertz electric fields exceeding 13 MV/cm at a 190 kHz repetition rate," *Opt. Lett.* **42**, 4367–4370 (2017).

18. B.-H. Chen, E. Wittmann, Y. Morimoto, P. Baum, and E. Riedle, "Octave-spanning single-cycle middle-infrared generation through optical parametric amplification in LiGaS<sub>2</sub>," *Opt. Express* **27**, 21306–21318 (2019).
19. K. Liu et al., "Multimicrojoule GaSe-based midinfrared optical parametric amplifier with an ultrabroad idler spectrum covering 4.2–16  $\mu\text{m}$ ," *Opt. Lett.* **44**, 1003–1006 (2019).
20. C. Manzoni, M. Först, H. Ehrke, and A. Cavalleri, "Single-shot detection and direct control of carrier phase drift of midinfrared pulses," *Opt. Lett.* **35**, 757–759 (2010).
21. T. Yamakawa, N. Sono, T. Kitao, T. Morimoto, N. Kida, T. Miyamoto, and H. Okamoto, "Long-term stabilization of carrier envelope phases of mid-infrared pulses for the precise detection of phase-sensitive responses to electromagnetic waves," *AIP Advances* **10**, 025311 (2020).
22. G. Andriukaitis, T. Balčiūnas, S. Ališauskas, A. Pugžlys, A. Baltuška, T. Popmintchev, M.-C. Chen, M. M. Mumane, and H. C. Kapteyn, "90 GW peak power few-cycle mid-infrared pulses from an optical parametric amplifier," *Opt. Lett.* **36**, 2755–2757 (2011).
23. N. Ishii, P. Xia, T. Kanai, and J. Itatani, "Optical parametric amplification of carrier-envelope phase-stabilized mid-infrared pulses generated by intra-pulse difference frequency generation," *Opt. Express* **27**, 11447–11454 (2019).
24. C.-H. Lu, Y.-J. Tsou, H.-Y. Chen, B.-H. Chen, Y.-C. Cheng, S.-D. Yang, M.-C. Chen, C.-C. Hsu, and A. H. Kung, "Generation of intense supercontinuum in condensed media," *Optica* **1**, 400–406 (2014).
25. J. E. Beetar, S. Gholam-Mirzaei, and M. Chini, "Spectral broadening and pulse compression of a 400  $\mu\text{J}$ , 20 W Yb:KGW laser using a multi-plate medium," *Appl. Phys. Lett.* **112**, 051102 (2018).
26. C.-H. Lu, T. Witting, A. Husakou, M. J. Vrakking, A. H. Kung, and F. J. Furch, "Sub-4 fs laser pulses at high average power and high repetition rate from an all-solid-state setup," *Opt. Express* **26**, 8941–8956 (2018).
27. P. He, Y. Liu, K. Zhao, H. Teng, X. He, P. Huang, H. Huang, S. Zhong, Y. Jiang, S. Fang, X. Hou, and Z. Wei, "High-efficiency supercontinuum generation in solid thin plates at 0.1 TW level," *Opt. Lett.* **42**, 474–477 (2017).
28. M. Bradler, P. Baum, and E. Riedle, "Femtosecond continuum generation in bulk laser host materials with sub- $\mu\text{J}$  pump pulses," *Appl. Phys. B* **97**, 561–574 (2009).
29. M. Nisoli, S. De Silvestri, and O. Svelto, "Generation of high energy 10 fs pulses by a new pulse compression technique," *Appl. Phys. Lett.* **68**, 2793 (1996).
30. S. Sartania, Z. Cheng, M. Lenzner, G. Tempea, Ch. Spielmann, and F. Krausz, and K. Ferencz, "Generation of 0.1-TW 5-fs optical pulses at a 1-kHz repetition rate," *Opt. Lett.* **22**, 1562–1564 (1997).
31. K. Reimann, R. P. Smith, A. M. Weiner, T. Elsaesser, and M. Woerner, "Direct field-resolved detection of terahertz transients with amplitudes of megavolts per centimeter," *Opt. Lett.* **28**, 471–473 (2003).
32. C. Kübler, R. Huber, S. Tübel, and A. Leitenstorfer, "Ultrabroadband detection of multi-terahertz field transients with GaSe electro-optic sensors: Approaching the near infrared," *Appl. Phys. Lett.* **85**, 3360–3362 (2004).
33. M. Ashida, "Ultra-Broadband Terahertz Wave Detection Using Photoconductive Antenna," *Jpn. J. Appl. Phys.* **47** 8221 (2008).
34. K. Yoshioka, I. Igarashi, S. Yoshida, Y. Arashida, I. Katayama, J. Takeda, and H. Shigekawa, "Subcycle mid-infrared coherent transients at 4 MHz repetition rate applicable to light-wave-driven scanning tunneling microscopy," *Opt. Lett.* **44**, 5350–5353 (2019).
35. R. Huber, A. Brodschelm, F. Tauser, and A. Leitenstorfer, "Generation and field-resolved detection of femtosecond electromagnetic pulses tunable up to 41 THz," *Appl. Phys. Lett.* **76**, 3191–3193 (2000).
36. K. Kaneshima, N. Ishii, K. Takeuchi, and J. Itatani, "Generation of carrier-envelope phase-stable mid-infrared pulses via dual-wavelength optical parametric amplification," *Opt. Express* **24**, 8660 (2016).